# Oxygen and hydrogen ion abundance in the near-Earth magnetosphere: Statistical results on the response to the geomagnetic and solar wind activity conditions

E. A. Kronberg,[1] S. E. Haaland,[1,2] P. W. Daly,[1] E. E. Grigorenko,[3] L. M. Kistler,[4] M. Fränz,[1] and I. Dandouras[5]

Received 27 June 2012; revised 20 September 2012; accepted 14 October 2012; published 8 December 2012.

[1] The composition of ions plays a crucial role for the fundamental plasma properties in the terrestrial magnetosphere. We investigate the oxygen-to-hydrogen ratio in the near-Earth magnetosphere from $-10\ R_E < X_{GSE} < 10\ R_E$. The results are based on seven years of ion flux measurements in the energy range ~10 keV to ~955 keV from the RAPID and CIS instruments on board the Cluster satellites. We find that (1) hydrogen ions at ~10 keV show only a slight correlation with the geomagnetic conditions and interplanetary magnetic field changes. They are best correlated with the solar wind dynamic pressure and density, which is an expected effect of the magnetospheric compression; (2) ~10 keV $O^+$ ion intensities are more strongly affected during disturbed phase of a geomagnetic storm or substorm than >274 keV $O^+$ ion intensities, relative to the corresponding hydrogen intensities; (3) In contrast to ~10 keV ions, the >274 keV $O^+$ ions show the strongest acceleration during growth phase and not during the expansion phase itself. This suggests a connection between the energy input to the magnetosphere and the effective energization of energetic ions during growth phase; (4) The ratio between quiet and disturbed times for the intensities of ion ionospheric outflow is similar to those observed in the near-Earth magnetosphere at >274 keV. Therefore, the increase of the energetic ion intensity during disturbed time is likely due to the intensification and the effective acceleration of the ionospheric source. In conclusion, the energization process in the near-Earth magnetosphere is mass dependent and it is more effective for the heavier ions.

**Citation:** Kronberg E. A., S. E. Haaland, P. W. Daly, E. E. Grigorenko, L. M. Kistler, M. Fränz, and I. Dandouras (2012), Oxygen and hydrogen ion abundance in the near-Earth magnetosphere: Statistical results on the response to the geomagnetic and solar wind activity conditions, *J. Geophys. Res.*, *117*, A12208, doi:10.1029/2012JA018071.

## 1. Introduction

[2] There are two major sources for the ion population in Earth's magnetosphere: the solar wind and the ionosphere.

[3] Hydrogen, helium and oxygen are the most abundant elements in the solar wind. According to measurements by SWICS on Ulysses, the oxygen abundance (H/O ratio) varies significantly between fast and slow solar winds, with mean values of 1500 and 2300, respectively [e.g., *von Steiger et al.*, 2010]. A direct entry of solar wind plasma into the magnetosphere is believed to occur mainly when the interplanetary magnetic field (IMF) is oriented southward. This leads to reconnection first at the dayside magnetopause and then in the magnetotail. Also, northward IMF results in reconnection at southern and northern high latitudes, facilitating the entry of solar wind plasma.

[4] The main source of oxygen in the magnetosphere is believed to be the terrestrial ionosphere [*Yau et al.*, 1984; *Lockwood et al.*, 1985; *Gloeckler et al.*, 1985; *Chappell et al.*, 1987; *Yau and Andre*, 1997; *Chappell et al.*, 2000; *Cully et al.*, 2003b; *Huddleston et al.*, 2005; *Moore and Horwitz*, 2007; *Kitamura et al.*, 2010], where oxygen ions are accelerated upward by electric fields parallel to the background magnetic field and pressure gradients. The ionospheric ions are either accelerated in the cusp/cleft region and then convected across the polar cap into the lobe [*Lockwood et al.*, 1985; *Kistler et al.*, 2010], or they come from the nightside aurora, which provides a fast feeding of

[1]Max-Planck Institute for Solar System Research, Katlenburg-Lindau, Germany.
[2]Department of Physics and Technology, University of Bergen, Bergen, Norway.
[3]Space Research Institute, Russian Academy of Sciences, Moscow, Russia.
[4]Space Science Center, University of New Hampshire, Durham, New Hampshire, USA.
[5]Institut de Recherche en Astrophysique et Planétologie, University of Toulouse, UPS-OMP, CNRS, Toulouse, France.

Corresponding author: E. A. Kronberg, Max-Planck Institute for Solar System Research, Max-Planck-Str. 2, Katlenburg-Lindau DE-37191, Germany. (kronberg@mps.mpg.de)


0148-0227/12/2012JA018071

$O^+$ ions in the near-Earth plasma sheet during the substorm expansion phase [*Yau et al.*, 1985; *Daglis and Axford*, 1996]. The kinetic energy of upflowing ions is typically a few tens of eV [*Yau and Andre*, 1997], whereas typical plasma sheet energies are much higher [e.g., *Lennartsson and Shelley*, 1986]. Centrifugal forces accelerate particles as they travel tailward along field lines [e.g., *Cladis*, 1986; *Nilsson et al.*, 2008, 2010], but the most significant energization will take place after the particles enter the plasma sheet.

[5] The accelerated plasma sheet particles are convected Earthward and populate the ring current which influences the transport in the radiation belts. The radiation belts are a key region for space weather studies, as their dynamics can induce damage to satellites and other space weather effects. Forecasting models based on radiation belt dynamics include the dynamics of the ring current. Additional ionospheric particles affect the background magnetic field, densities, temperature and convection electric field, and therefore lead to, e.g., changes in the ring current [*Welling et al.*, 2011]. It is challenging to include the heavy ion contribution in numerical studies of the ring current [e.g., *Glocer et al.*, 2009; *Welling et al.*, 2011] or radiation belt models. Knowledge about the ion composition and its dependence on solar wind and magnetospheric conditions is important for defining the boundary conditions in such simulations.

[6] A number of earlier studies have demonstrated that the abundance of oxygen in the ring current region can change significantly with geomagnetic activity. *Sharp et al.* [1981] have reported measurements of oxygen in the energy range 0–17 keV/e at distances between 11 and 23 $R_E$ downtail by the ISEE 1 spacecraft. *Gloeckler et al.* [1985] analyzed for the first time the ion composition measurements of the ring current during the storm time using AMPTE/CCE spacecraft data in the energy range ~1 to 300 keV/e at L values between ~3 and 6.5. They suggested that large changes in the $O^+$ number and energy densities implied an injection of energetic ionospheric ions. *Hamilton et al.* [1988], using AMPTE particle measurements, found an event in which the $O^+$ dominates $H^+$ in the ring current during a large magnetic storm. A later study by *Daglis et al.* [2000] established a connection between $O^+$ (50–426 keV, measured by CRRES) enhancements during storms and substorm activities in the inner magnetosphere at L ~ 7. Another, more extensive study by *Fu et al.* [2002], using CRRES observations, has shown that not all injection events have the same ion composition. Their statistical results demonstrated that about 73% of all the events were rich in oxygen ions and the rest have very low admixtures of oxygen. Events without oxygen ions were found to be mainly correlated with weak geomagnetic activity conditions.

[7] The abundance of oxygen in the magnetotail's plasma sheet can vary significantly with geomagnetic activity. *Moebius et al.* [1987] showed that the spectra harden in the magnetotail's plasma sheet during substorm, with a larger energy increase for $O^+$ than for $H^+$, i.e., the $O^+/H^+$ ratio also increases with energy. For this case study they used observations from AMPTE/IRM which resolved the ion composition of the suprathermal population (10–230 keV/e). *Kistler et al.* [1990] used AMPTE/IRM observations to compare spectral changes at 15–19 $R_E$ (tail) and 7–9 $R_E$ (inner magnetosphere, night side). They found that the spectral changes were very similar at both locations. *Kistler et al.* [1994] investigated how the flux of the energetic particles observed by the AMPTE/IRM decreases after the initial particle "injection". These observations show that the decay rate is organized by total energy, energy per charge and velocity. In a statistical study, *Nosé et al.* [2009] used 16 years of Geotail data in order to look at the suprathermal ion composition in the plasma sheet in the range $-100R_E < X_{GSM} < -8R_E$. They investigated the correlation between the $O^+/H^+$ ratio and solar activity using the F10.7 index and with the geomagnetic activity using the Kp index. They found that physical processes in the plasma sheet are expected to be much different during solar minimum and solar maximum, because the Alfvén velocity changes significantly between these two solar activity regimes. More recently, ion composition data from the CIS/CODIF instrument on the Cluster spacecraft were used to study $O^+$ and $H^+$ bulk content (0–40 keV/e) in the plasma sheet within 15–19 $R_E$ as a function of solar activity and geomagnetic activity [*Mouikis et al.*, 2010]. They found that the $O^+$ density were strongly dependent on these parameters.

[8] In this paper, we present a comprehensive study of the $O^+$ and $H^+$ abundance in the plasma sheet of the near-Earth magnetosphere (from $-10\ R_E < X_{GSE} < 10\ R_E$). The data are obtained from seven years of particle measurements by the Cluster satellites. We compare the characteristic behavior of the ions at ~10 keV and at 274–955 keV to different solar wind and geospace activity factors.

[9] The novelty of this study is a combination of (a) the extensive spatial region coverage of the near-Earth magnetosphere, (many previous studies either focused on the magnetotail region or were mainly case studies in the near-Earth region only); (b) energy range, as no extensive statistical study has been done so far with energies up to ~955 keV; (c) a comparative analysis of ion intensities at different energies, namely at ~10 keV and from 274 keV to ~955 keV; (d) the advantage of having more accurate parameters of the solar-terrestrial coupling which became available during the last 15 years.

[10] We can for the first time investigate the details of how the near-Earth hydrogen and oxygen populations depend on the geomagnetic and solar wind activity.

[11] The paper is organized as follows: In section 2, we give a brief overview of the Cluster spacecraft, the RAPID and CIS ions spectrometers and their data products. In section 3, we explain how we process the data and derive the $O^+/H^+$ ratio. Section 4 presents the observations and shows how the $O^+$ and $H^+$ abundance varies with different parameters controlling the dynamical state of the magnetosphere such as solar wind conditions and also geomagnetic disturbance level. Section 5 discusses the results and related physical processes. Section 6 summarizes the observations.

## 2. Data and Instrumentation

[12] The results presented in this study are primarily based on in-situ measurements from the Cluster quartet of spacecraft. The Cluster mission comprises four identical spacecraft flying in a tetrahedron-like formation. More information about the Cluster mission and instrumentation is given in *Escoubet et al.* [1997]. In this paper we have used data from the SC4 spacecraft, since this gives the best data return for our purpose.

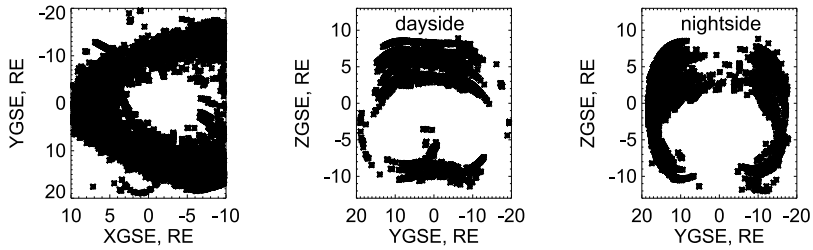


**Figure 1.** Maps of the location of the energetic oxygen observations, from left in $XY_{GSE}$, $YZ_{GSE}$ dayside ($X_{GSE} > 0$) and $YZ_{GSE}$ nightside ($X_{GSE} \leq 0$) planes.

[13] For the period covered by this study Cluster was in a nearly 90° inclination elliptical orbit with apogee around 19.6 $R_E$ and perigee around 4 $R_E$. Due to spacecraft orbits in the near-Earth region our observations mainly cover the dawn and dusk flanks and the dayside plasma sheet, mainly the north part, see Figure 1. This figure shows maps of the energetic $O^+$ observations, projected into $XY_{GSE}$, $YZ_{GSE}$ dayside and $YZ_{GSE}$ nightside planes, respectively. This coverage allows us to study the transport of ions from the tail region around the Earth.

[14] In addition to the in-situ Cluster observations, we also use solar wind magnetic field and plasma data and geomagnetic disturbance indices to check dependencies and correlations.

[15] In this study, we use the AE and Dst indices and not the Kp index as, e.g., *Nosé et al.* [2009] or *Mouikis et al.* [2010] because they are more precise (the Kp index has a 3 hours cadence, while the AE and Dst indices have higher time resolution) and have a more direct physical meaning. The Dst index primarily reflects slow (hours) magnetic perturbations caused mainly by ring current enhancements, whereas the AE index reflects short time (minutes) perturbations at high latitudes caused by variations in field-aligned current due to plasma sheet processes such as bursty bulk flow activity.

### 2.1. Cluster Particle Measurements

[16] We use ion measurements from two different sensors onboard Cluster. Energies above 30 keV are covered by RAPID: the Research with Adaptive Particle Imaging Detector [see *Wilken et al.*, 2001], whereas the lower part of the energy range (energies below 40 keV) is covered by CIS: the Cluster Ion Spectroscopy instrument [see *Rème et al.*, 2001].

#### 2.1.1. Energetic Ion Fluxes From RAPID

[17] The RAPID Imaging Ion Mass Spectrometer (IIMS) consists of three identical detector heads and use a combination of time-of-flight and energy measurements to classify and bin the incident particles. The three sensors cover 180° in polar angle, and by utilizing the spacecraft spin, RAPID/IIMS provides the distribution of ions with complete coverage of the unit sphere in phase space. Due to a degradation of the central heads on the ion sensor on all spacecraft during the early phase of the mission, only a limited part of the full 3D distribution is available during later stages, however. Since our purpose is to investigate the statistical abundance of two distinct ion species in a particular plasma region, we are not dependent on any 3D abilities, but integrate over all directions to get an omnidirectional flux. Except for extremely anisotropic distributions, the lack of sensitivity in the central sensor does not play any major role [*Kronberg et al.*, 2010].

[18] RAPID/IIMS allows for discrimination of various ion species by utilizing time-of-flight and energy information of each incident particle. The resolution of the instrument makes it possible to group ions into three categories; protons ($H^+$ atomic mass unit 1), helium (He, atomic mass units 2–4) and a common group of heavy ions (atomic mass units 14–16). This latter group is dominated by oxygen, but the mass resolution does not allow for distinction between oxygen, carbon and nitrogen. This group is therefore commonly refereed to as the CNO group. The energy ranges are 28 keV–4 MeV for protons, 137 keV–3.8 MeV for helium and 274 keV–4 MeV for the CNO group. No information about charge state is possible. For simplicity, we will simply refer to the ratio $O^+/H^+$ in case of RAPID data, although, we mean the CNO mass group and hydrogen, respectively.

[19] The time resolution of the RAPID omnidirectional data is 1 spin (~4 s), but since the count rates are often very low, we have used 1 minute averages in this study.

#### 2.1.2. Moments and Particle Measurements From CIS

[20] CIS consists of two sensors. In this paper we use data from the Composition and Distribution Function (CODIF) instrument to calculate an omnidirectional flux as done for RAPID. The energy range for CIS is 0.03–40 keV per charge. In addition to the omnidirectional proton and $O^+$ fluxes, we also utilize plasma moments from the CODIF sensor.

[21] As for RAPID we use 1 minute averages and put them on the same timeline as the rest of the data set. Plasma moments are used to identify the plasma region and to filter the data. The CIS instrument has several sensitivity modes, automatically switched in-flight in order to achieve optimal sensitivity and resolution for a particular plasma region. To avoid errors introduced by mode shifting and non-optimal modes we only use data from the so-called magnetospheric mode 13 (see details in *Rème et al.* [2001] and *Dandouras et al.* [2006]).

[22] $O^+$ measurements by CIS can be slightly contaminated by protons (the major species). The contamination of $H^+$ into $O^+$ is about 0.1–0.3% (depending on energy and on a particular mode) for low count rates (e.g. in the magnetosphere) for ~10 keV ions. In order to compensate for this contamination of oxygen by protons during active time periods, we calculate the oxygen intensities as follows:

**Table 1.** Lower Thresholds of Energy Channels for Protons and Oxygen for RAPID[a]

| Channel | Energy Range $H^+$ (keV) | Energy Range $O^+$ (keV) |
|---|---|---|
| 1 | 28–64[b] | 84[c] |
| 2 | 75 | 274 |
| 3 | 92 | 414 |
| 4 | 160 | 498 |
| 5 | 374 | 638 |
| 6 | 962 | 948 |
| 7 | 1885 | 1414 |
| 8 | —[d] | 2539 |
| Upper | 4007 | 4046 |

[a]Note that energy channels for $H^+$ and $O^+$ are not overlapping. To make the $O^+/H^+$ ratio meaningful, we therefore fit a spectrum and derive an additional $H^+$ energy channel for RAPID, see Appendix A.
[b]Energy gap between hydrogen 1 & 2.
[c]CNO channel 1 contaminated at times, suppressed.
[d]The 8th channel is not accessible for hydrogen.

$j^{O^+} = j_m^{O^+} - j^{H^+} \cdot 0.001$, where $j_m^{O^+}$ and $j^{H^+}$ are the measured oxygen and proton intensities, respectively.

## 3. Methodology

### 3.1. Calculation of the $O^+/H^+$ Ratio

[23] Our purpose is to compare $O^+/H^+$, namely, the ratio between intensities which are proportional to the number fluxes of $O^+$ and $H^+$ (1/cm$^2$ sr s keV) in two energy ranges. This ratio is equal to the ratio between integral fluxes if the energy range is identical for the two species. To be able to identify any spectral changes, we use two different energy ranges, ~10 keV (8.1 to 10.3 keV) and the energy band 274–955 keV. These energy bands are somewhat arbitrarily chosen, and are a compromise between the energy binning of the two instruments and sufficient statistics. We take a wide energy band for the energetic ions since the measurements of ions at these energies have relatively low count rates and wide energy channel divisions. As we do not consider details of any particular acceleration process but only the response of the particle population to the different geomagnetic and solar wind activity, the use of the wide energy range of the energetic ions is justified in this study.

[24] For the CIS instrument, the ratio between the number fluxes of $O^+$ and $H^+$ is based on the same energy range; since the energy channels are similar for protons and oxygen. For RAPID, however, the energy binning for $O^+$ and $H^+$ have different thresholds, see energy ranges listed in Table 1. The details on how the RAPID energy channels were rebinned for the most effective intensities comparison are described in Appendix A. These RAPID integral intensities ($J^{H^+}$ and $J^{O^+}$) are used in the current study.

### 3.2. Construction of Plots

[25] Figures 2 to 6 show median intensities for protons and oxygens in two different energy bands versus the respective geomagnetic or solar wind parameter. The plots are constructed from data accumulated in the plasma sheet region, defined by plasma beta value in the range 0.1–10 [*Baumjohann et al.*, 1989]. We have excluded observations where the magnetic field component $B_z$ was negative in order to avoid the cusp region. Furthermore, we limit our study to the near-Earth magnetosphere, i.e. distances $-10\ R_E < X_{GSE} < 10\ R_E$. We also exclude data from radial distances <6 $R_E$, as the sensors can be affected by pileup effects from both penetrating particles (e.g. during solar proton events) and high count rates.

[26] To minimize the effect of skewed distribution, we use median rather than mean values of the distribution functions. For the same reason, statistical spreads are given as median absolute deviations (MAD), [see, e.g., *Venables and Ripley*, 1999]. Median value and MAD are less sensitive to non-normal distribution functions than the mean value and standard deviation. In order to determine whether differences between values are significant, confidence interval (CI) error bars are given in Figures 2 to 6: $CI = SE \cdot t_{n-1}$, where $t_{n-1}$ is the $t$-distribution with $n$ degrees of freedom, $SE = \sigma/\sqrt{n}$ is standard error, where $\sigma$, the standard deviation, was calculated in this case as: $\sigma = 1.4826 \cdot MAD$ [*Huber*, 1981].

[27] The $O^+/H^+$ ratio is defined as the ratio between median values of the $O^+$ and $H^+$ intensities. Correspondingly, errors for the $O^+/H^+$ ratio are calculated as: $CI_{O^+/H^+} = \sqrt{(CI_{O^+}/O^+)^2 + (CI_{H^+}/H^+)^2} \cdot O^+/H^+$. Each value shown in Figures 2–6 contains at least 100 measurements.

[28] The histogram ranges for Dst, AE, solar wind density and solar wind pressure are defined as follows. The distributions of these parameters are skewed. In order to avoid outliers, which would take attention away from the more typical values we (1) compute quartiles of the distribution; (2) define interquartile range (IQR) between first quartile, Q1, and third quartile, IQR = Q3–Q1; (3) use the 1.5·IQR rule for outliers, which approximately corresponds to $3\sigma$. This will lead to the histogram ranges between Q1–1.5·IQR and Q3 + 1.5·IQR. The behavior of the oxygen and proton intensities are rather complicated at values which are larger than $\pm 3\sigma$. As an exception we extended the range for the Dst from −70 nT to −100 nT, in order to cover the whole range for moderated storms.

## 4. Results

[29] Below, we present and discuss how the $O^+$, $H^+$ intensities and $O^+/H^+$ ratio depend on respective parameters of the solar-terrestrial coupling in more detail.

### 4.1. Response to Magnetic Activity

#### 4.1.1. Geomagnetic Storms

[30] The interaction between a solar wind shock wave and/or an interplanetary magnetic cloud with the terrestrial magnetic field can lead to the phenomena called magnetic storms during which the horizontal component of the Earth's magnetic field decreases dramatically. This decrease is reflected by the Dst index.

[31] The response of the ion intensities to the changes in the Dst index is shown in Figure 2 and summarized in Table 2. The intensity of protons at ~10 keV and at >274 keV increases approximately in the same manner with decrease of Dst index down to −100 nT (the maximum intensity is ~2 times higher than the minimum intensity). Oxygen intensities at both energies show more dramatic changes with Dst index. Intensities are up to 30 times higher between the minimum to the maximum. However, during weak (Dst

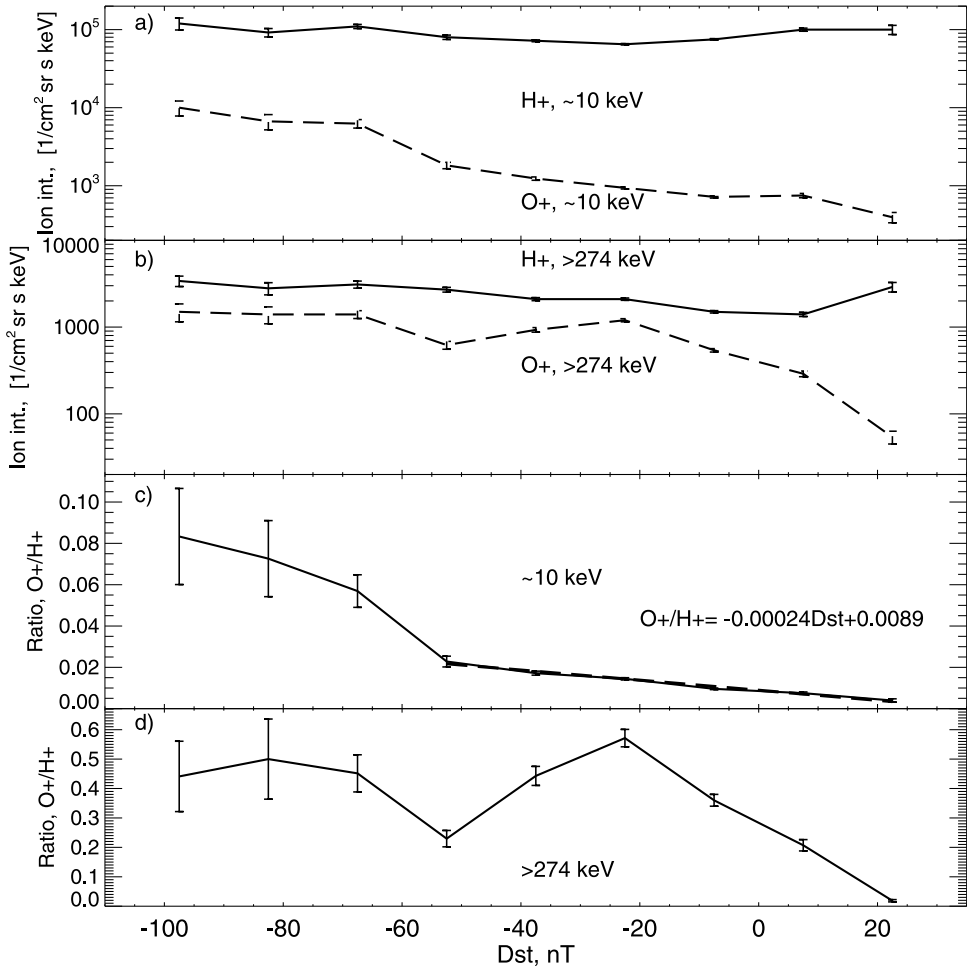


**Figure 2.** Dependencies on Dst index of (a) proton and oxygen intensities at ~10 keV, (b) proton and oxygen intensities for >274 keV, (c) ratio $O^+/H^+$ for intensities at ~10 keV and (d) ratio $O^+/H^+$ for intensities at >274 keV. The dashed line in Figure 2c indicates a linear fit to the ratio values. Error bars indicate 99% confidence intervals.

below −30 nT) and moderate (Dst below −50 nT) magnetic storms, the ratio $O^+/H^+$ is affected more strongly at ~10 keV. Since the ~10 keV $O^+$ intensity grows significantly (5 times) at Dst from −30 to −100 nT, compared to no change of $O^+/H^+$ ratio at >274 keV. At the higher energies, the intensities of both species grow together during weak and moderate storms, therefore, the $O^+/H^+$ ratio does not clearly change. This agrees with *Ono et al.* [2009] who found that during dipolarization associated with substorms the energy density of energetic oxygen does not always increase. However, we see a significant growth of the >274 keV oxygen, and of $O^+/H^+$ ratio during the growth phase, from 15 to −30 nT. Therefore, a significant amount of >274 keV oxygen is effectively accelerated during a storm growth phase.

[32] At positive Dst > 15 nT the intensity of >274 keV protons is clearly higher compared to that at Dst ≃ 0. This is expected as positive Dst values are associated with a compression of the magnetopause which can lead to a drift shell displacement. An enhanced intensity of ~10 keV $H^+$ is observed for positive values of Dst. The effect is not observed in the $O^+$ intensity, though.

[33] Based on the observations, we can define linear functional dependence between the $O^+/H^+$ ratio and disturbance level (from −60 to 30 nT):

$$O^+/H^+ = -2.4 \cdot 10^{-4} \times \mathrm{Dst[nT]} + 8.9 \cdot 10^{-3}.$$

The dependency is constructed using a linear least squares fit.

[34] We find a weak correlation between proton intensity (both at ~10 keV and >274 keV) and Dst. This is consistent with results reported by, e.g., *Nosé et al.* [2009] and *Mouikis et al.* [2010]. Also consistent with our results, *Mouikis et al.* [2010] found significantly stronger correlation of oxygen intensities and geomagnetic activity in the magnetotail region.

#### 4.1.2. Response to Magnetotail Processes

[35] Processes in the magnetotail due to e.g. magnetospheric substorms and bursty bulk flows causing enhanced field-aligned currents leading to auroral electrojet activity reflected in the AE index.

[36] Figure 3 shows the response in $H^+$ and $O^+$ intensities to these processes. The increase in the AE index is associated with an exponential growth by a factor 4 (from the

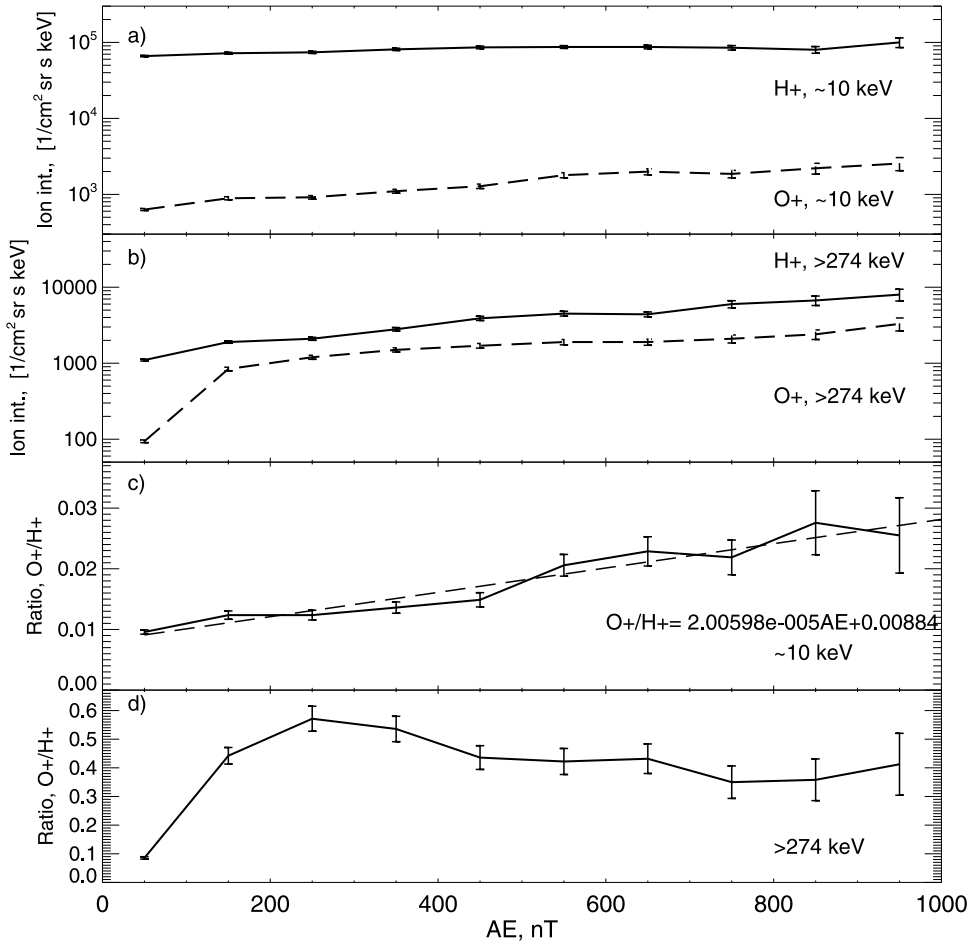


**Figure 3.** Dependencies on AE index of (a) proton and oxygen intensities at ~10 keV, (b) proton and oxygen intensities at >274 keV, (c) ratio $O^+/H^+$ for intensities at ~10 keV and (d) ratio $O^+/H^+$ for intensities at >274 keV. The dashed line in Figure 3c indicates a linear fit to the ratio values. Error bars indicate 99% confidence intervals.

minimum to the maximum) of the ~10 keV oxygen intensities. The ~10 keV protons only show a slight increase with AE index, (maximum value ~1.5 time higher than the lowest value). As above, we can now establish an empirical functional relation between $O^+/H^+$ ratio and AE index for ~10 keV ions

$$O^+/H^+ = 2 \cdot 10^{-5} \times AE[nT] + 8.8 \cdot 10^{-3}.$$

The increase of the $O^+/H^+$ ratio at ~10 keV energies means that the oxygen is accelerated up to these energies more effectively than protons, although sources of their acceleration have to be different. The study by *Ono et al.* [2009] shows similar results: acceleration of $O^+$ at energies of 9 to 36 keV/e during substorms (by electric fields induced by magnetic field fluctuations whose frequencies are close to the gyrofrequencies of ions) is more effective than of $H^+$. Event studies by *Zong et al.* [2008, 2009] have shown that bursty bulk flows can be responsible for supply of the ionospheric oxygen into the near-Earth magnetosphere.

[37] Proton intensities at >274 keV show an exponential increase with AE. Intensities are ~8 times higher for high AE values. A similar dependence between AE and >274 keV oxygen intensities are also observed, although the slope has a break at 150–250 nT (strong growth before and moderate after). The highest intensities of >274 keV oxygen, at high AE values are about 33 times higher than the lowest intensities.

[38] The effect of substorms on the abundance of the $O^+$ ions relative to protons is larger at ~10 keV, since the $O^+$ intensity increases more strongly than $H^+$. At higher energies, the intensities of the two species seem to increase approximately in the same way starting from AE ≃ 200 nT. This again agrees with results obtained by *Ono et al.* [2009] who did not find a clear correlation between substorm-associated dipolarizations and effective $O^+$ acceleration for ions in the energy range 56–212 keV/e. However, our results show a significant increase in intensities of >274 keV oxygen from quiet (AE ≃ 0–100 nT) to more disturbed times (AE ≃ 150–250 nT). Therefore, a significant amount of >274 keV oxygen is effectively accelerated during weak/moderate substorms or during a substorm growth phase.

### 4.2. Response to Solar Wind Conditions

#### 4.2.1. Response to IMF Direction

[39] The response of the ion intensities to the changes in IMF direction is shown in Figure 4. The IMF direction is

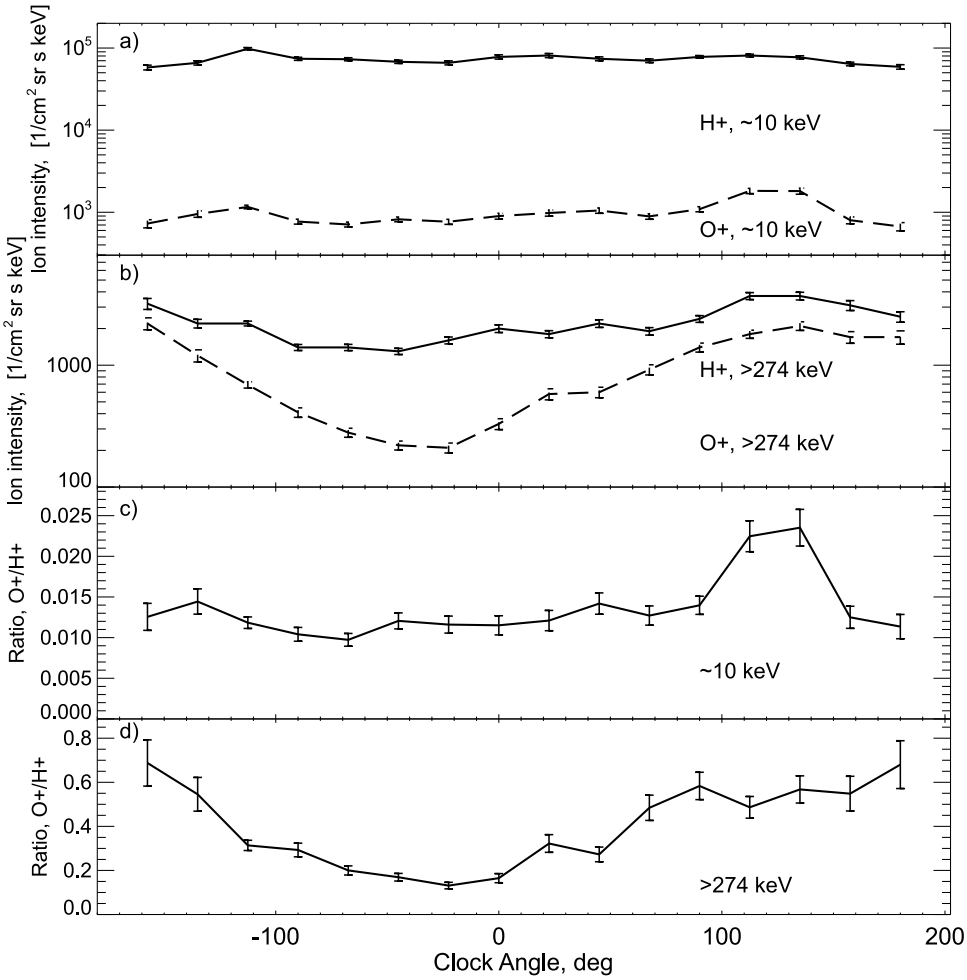


**Figure 4.** Dependencies on Clock Angle of (a) proton and oxygen intensities at ~10 keV, (b) proton and oxygen intensities at >274 keV, (c) ratio $O^+/H^+$ for intensities at ~10 keV and (d) ratio $O^+/H^+$ for intensities at >274 keV.

represented by the clock angle (CA) defined as the angle between $Z_{GSE}$ and the projection of IMF into the $YZ_{GSE}$ plane.

[40] When IMF Bz is negative (i.e. southward IMF), the coupling to the Earth's geomagnetic field is strongest. Southward interplanetary magnetic conditions are typically associated with geomagnetic storm activity.

[41] In order to take into account that the changes in particle population do not immediately respond to changes in IMF direction, we only use those measurements during periods where IMF was reasonably stable for at least 30 min.

[42] The intensity of ~10 keV protons increases slightly at the IMF clock angle, −115° in ~1.5 times from the minimum to the maximum. For the oxygen intensities the increases are observed at −115° and 125°, in ~2.5 times from the minimum to the maximum.

[43] High energy particles (energy >274 keV) are much more sensitive to IMF clock angle variations, especially oxygen ions. The oxygen and proton intensities at >274 keV are a factor of 10 and 3 higher for southward IMF, respectively. We find a strong positive correlation between the intensities of >274 keV $O^+$, $H^+$, the $O^+/H^+$ ratio and the IMF direction. The energetic ion intensities seem to be correlated with the "openness" of the magnetosphere or change of the clock angle toward the southward direction. However, during the most southward IMF (and dawnward) the acceleration ceases to be effective, the $O^+/H^+$ ratio does not show significant changes.

[44] Since RAPID does not discriminate between charge states, oxygen of solar wind origin (with higher charge states) might explain the strong correlation with IMF clock angle. To check this, we compared our intensities with corresponding intensities of high charge state oxygen, with clear solar wind origin, measured by *Kremser et al.* [1987] in the inner magnetosphere using the AMPTE/CHEM data set. Their results indicate that intensities of high charge state oxygen were about one order of magnitude lower than our RAPID results. Hence, we think that our observations are primarily of ionospheric origin. The effect of IMF orientation is significantly larger for the intensity ratio of the $O^+$ ions to protons at >274 keV than at ~10 keV. These all suggest a connection between the energy input to the magnetosphere related to the change of clock angle and the energization of $O^+$ to high energies (>274 keV).

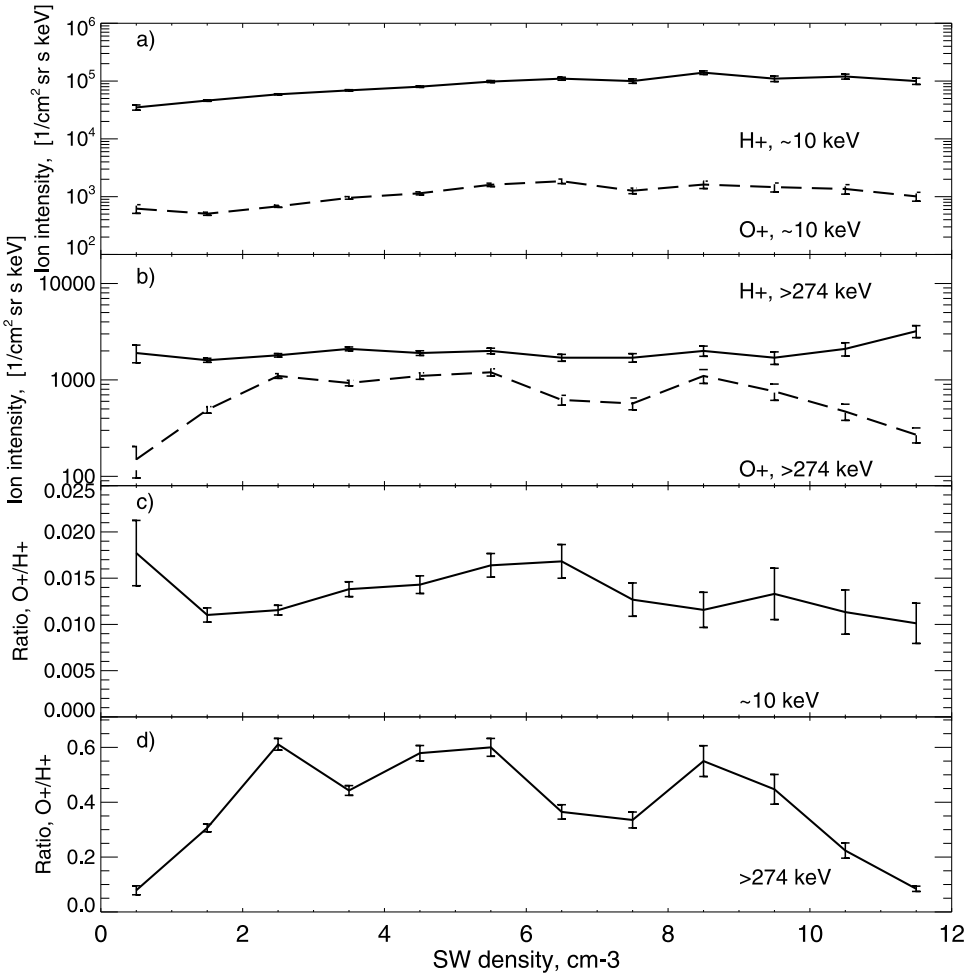


**Figure 5.** Dependencies on solar wind density of (a) proton and oxygen intensities at ~10 keV, (b) proton and oxygen intensities at >274 keV, (c) ratio $O^+/H^+$ for intensities at ~10 keV and (d) ratio $O^+/H^+$ for intensities at >274 keV.

#### 4.2.2. Solar Wind Density and Pressure

[45] The response of the ion intensities to changes in solar wind density and pressure is shown in Figures 5 and 6, respectively. Intensities of ~10 keV oxygen and protons are almost exponentially increasing with solar wind density, (by a factor of ~4 for $H^+$ and a factor of ~3 for $O^+$). For energies >274 keV, we do not see any clear dependence on the solar wind density.

[46] The ~10 keV protons and oxygen show almost exponential increase (by a factor ~4) with the solar wind dynamic pressure. The proton intensities at >274 keV increase (by a factor of ~5) with the solar wind pressure. There is no clear general dependency of the >274 keV oxygen intensities on the solar wind pressure. However, for >274 keV $O^+$, we observe a ~40 fold increase between ~0.5 nPa to 1.75 nPa. At these solar wind pressure values, the energetic oxygen is accelerated more effectively than energetic protons. This is also supported by the fact that in ~10 keV oxygen such a tendency is not observed. From ~1.75 nPa to 3 nPa the intensity of the >274 keV oxygen and protons becomes almost equal.

[47] Statistically, the solar wind density strongly correlates with the plasma sheet density [*Borovsky et al.*, 1998]. This is seen for the ~10 keV protons. For ~10 keV protons we find a strong correlation between intensity and the solar wind density and pressure.

[48] The increase of ~10 keV $O^+$ intensities is well correlated with the increase of the solar wind dynamic pressure. This is in agreement with earlier studies, e.g., by *Cully et al.* [2003a] and *Nosé et al.* [2003] who found that the ionospheric outflow is strongly affected by the solar wind dynamic pressure. Also in a study by *Echer et al.* [2008], it was shown that a shock compression can lead to enhanced inflow of the oxygen ions into the near-Earth magnetosphere. However, this can be also compression effects (see section 5.5).

[49] Intensities of ~10 keV oxygen ions show clear dependencies on solar wind dynamic pressure, as this energy is closer to source energies. This is not the same for energetic ions which are not closely related with outflow energies and require stronger acceleration. The observed prominent increase in the oxygen intensities for solar wind dynamic pressure up to 1.5 nPa is more likely related to acceleration mechanisms due to the thinning of the plasma sheet (see section 5.4). The largest increase in the energetic

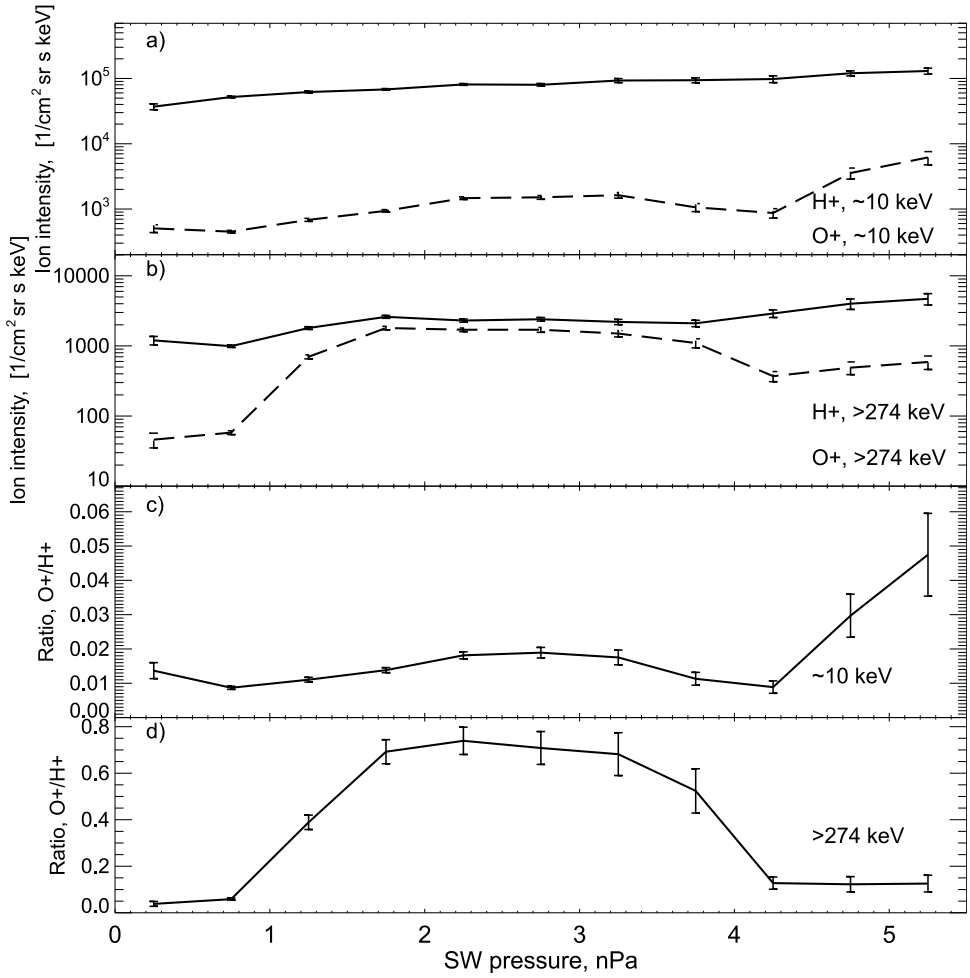


**Figure 6.** Dependencies on solar wind pressure of (a) proton and oxygen intensities at ~10 keV, (b) proton and oxygen intensities at >274 keV, (c) ratio $O^+/H^+$ for intensities at ~10 keV and (d) ratio $O^+/H^+$ for intensities at >274 keV.

particle intensities is seen during the transition period between quiet and disturbed times.

## 5. Discussion

### 5.1. Comparison to Other Observations

[50] Our energy density results listed in Table 3 (see calculations in Appendix A, equation (A1)) are comparable to the observations in the near-Earth plasma sheet made by, e.g., *Gloeckler et al.* [1985], *Hamilton et al.* [1988] and *Nosé et al.* [2001]. We do not observe the dramatic differences between quiet and disturbed times reported in these earlier studies, though. A possible reason is that we have used median values rather than mean values, and thus avoid effects of outliers and strongly scattered distributions. Also, the definitions of quiet and disturbed times, are based on AE index and Dst indices and differs from earlier studies. One could notice that the difference between quiet and disturbed times for the ~10 keV ions is stronger when using the Dst index as definition. Taking even more negative values of Dst will lead to the higher $O^+/H^+$ ratios. Therefore, the dynamics of the ~10 keV particles in the near-Earth magnetosphere is more strongly correlated with the Dst index.

### 5.2. Comparison to Ionospheric Outflow Observations

[51] Ion outflow rates (at 0.01–17 keV) can vary by a factor of 30 between quiet and very disturbed periods [*Yau et al.*, 1985]. Our result shows that the >274 keV oxygen intensity is about 33 times higher during very disturbed periods than during quiet time (here AE index is used). For comparison, the ~10 keV $O^+$ intensity increases a factor 4 between quiet and very disturbed times. Acceleration of ~10 keV oxygen seems to be more effective during disturbed times, while for >274 keV oxygen acceleration primary occurs during transitions from quiet to disturbed periods. Such slope break between quiet and disturbed states is not observed in the ionospheric $O^+$ outflow [*Yau et al.*, 1985; *Cully et al.*, 2003a].

[52] For protons, the intensities of ~10 keV ions are only slightly different during disturbed periods than during quiet times. The intensity of protons with energies >274 keV increases by a factor of about 8 between quiet and disturbed times. For comparison, for auroral and polar protons outflow

**Table 2.** Response of Ion Intensity to Changes in the Dst Index

| Particles | Compression[a] Dst > 15 nT[f] | Growth Phase[b] −30 < Dst < 15 nT | Weak-Moderate[c] −105 < Dst < −30 nT | Quiet-Storm Time[d] −105 < Dst < 0 nT | Min-Max[e] |
|---|---|---|---|---|---|
| $H^+$ ∼10 keV | no change | no change | +1.6x[g] | +1.4x | +2x |
| $O^+$ ∼10 keV | −2x[g] | +1.5x | +8x | +14x | +13x |
| $O^+/H^+$ ∼10 keV | −2x | +1.7x | +5x | +10x | +22x |
| $H^+$ >274 keV | +2x | +1.5x | +1.6x | +2.3x | +2.4x |
| $O^+$ >274 keV | −8x | +3x | +1.6x | +3.6x | +30x |
| $O^+/H^+$ >274 keV | −16x | +2x | no change | +1.6x | +30x |

[a]Difference between ion intensities at ∼22.5 nT and ∼0 nT (here and further, the mean values of the corresponding bins), namely during magnetospheric compression.
[b]Difference between ion intensities at ∼0 nT and ∼−22.5 nT, namely between beginning and end of the growth phase.
[c]Difference between ion intensities at ∼−37.5 nT and ∼−97.5 nT, namely between weak and moderate storms.
[d]Difference between ion intensities at ∼0 nT and ∼−97.5 nT, namely between quiet and storm time.
[e]Difference between minimum and maximum ion intensities in Figure 2.
[f]This value and corresponding values in the next columns are the thresholds of the ranges.
[g]Note that "−*x" is decrease in * times and "+*x" is increase in * times.

an increase of the order of 5 was reported by *Yau et al.* [1985].

[53] The ratio between quiet and disturbed times for the ion ionospheric outflow is higher than those observed in the near-Earth magnetosphere at ∼10 keV but similar to those observed at >274 keV. These appears to be a connection between the energetic ion intensities and ion outflow that changes with geomagnetic activity. The fact that the ratios between quiet and disturbed times are higher for the more energetic and heavier particles means that the ions are more effectively accelerated up to these energies. This is consistent with explanation by *Moebius et al.* [1987] and many other studies thereafter, that the acceleration process in the near-Earth magnetosphere is mass dependent, as it is more effective for the heavier particles.

### 5.3. Response of Protons to Geomagnetic Activity and Solar Wind Conditions

[54] As shown in section 4.2.1, the intensity of ∼10 keV protons does not seem to be directly affected by dayside reconnection. Response to IMF direction would be expected, though, as it is likely to be associated with dayside reconnection and then consequent transfer of the solar wind ions into the magnetosphere and subsequent acceleration. By the same token, magnetic storms and substorm activity are typically also related to the dayside reconnection. In addition storms and substorms are typically associated with enhanced outflow. As a consequence, more ions would be energized in the magnetosphere. Still, the correlation between the ∼10 keV proton intensities on one hand, and geomagnetic activity, solar wind dynamic pressure and clock angle on the other hand is less pronounced than for the ∼10 keV oxygen (see sections 4.1.1, 4.1.2, and 4.2.1).

[55] These observations can be explained as follows. Heavier ions ($O^+$) require additional forces such as electric fields, wave activity or stronger gradients in pressure and temperature to escape from the ionosphere. These processes are primarily driven by enhanced dayside reconnection and the subsequent processes reflected by increased disturbance levels. Protons, on the other hand, with their much lower escape energies, are not so dependent on these external forces. Solar illumination alone suffices to extract a significant number of light ions from the ionosphere. Therefore, the strong dependence on the disturbance parameters of the ∼10 keV protons is not observed.

### 5.4. Changes During Growth Phase

[56] Why would we expect an increase in energetic oxygen intensities during the transition period between quiet and disturbed times (substorm growth phase)? The increased solar wind pressure (or loading of the energy during Dungey cycle) can lead to the plasma sheet thinning [e.g., *Sauvaud et al.*, 1996] and therefore to a more effective acceleration of the heavy ions [e.g., *Ganguli et al.*, 1995]. There are different regimes of particle motion in the plasma sheet derived by *Büchner and Zeleny* [1986]. According to their work the particles are accelerated most effectively when parameter $\kappa = \sqrt{\frac{r_{curv}}{r_g}} \sim 1$, where $r_{curv}$ is the radius of magnetic field curvature and $r_g$ is ion gyroradius. Under these

**Table 3.** $O^+/H^+$ Ratios of Energy Density Depending on the Disturbance Level

| Satellite/Instrument | Energy Range (keV) | $O^+/H^+$, Energy Density | |
|---|---|---|---|
| | | Quiet Time | Disturbed Time |
| Cluster/RAPID | 274 keV–∼955 keV | 0.22 ± 0.12[a], 0.72 ± 0.44[b] | 1.04 ± 1.33[a], 1.11 ± 1.35[b] |
| Cluster/CIS | ∼10 keV | 0.038 ± 0.0081[a], 0.034 ± 0.0031[b] | 0.083 ± 0.038[a], 0.2 ± 0.12[b] |
| AMPTE/CCE[c] | 1–310 keV | 0.03 | 0.34 |
| AMPTE/CCE[d] | 1–310 keV | 0.01 | 0.61 |
| Geotail/EPIC[e] | 9–210 keV | 0.05–0.1 | 0.2–0.6 |

[a]Quiet (AE < 100 nT) and disturbed conditions (AE > 300 nT) are based on the AE index.
[b]Quiet (Dst ∼ 0 nT) and disturbed (Dst is between −100 and −30 nT) are determined based on the Dst index.
[c]Measurements taken from *Gloeckler et al.* [1985].
[d]Measurements taken from *Hamilton et al.* [1988].
[e]Measurements taken from *Nosé et al.* [2001].

conditions the particle trajectories become stochastic and particles are effectively accelerated by quasi-stationary dawn-dusk electric fields. A decrease in plasma sheet thickness, e.g. in response to an increase of the lobe magnetic field, will lead to larger region where stochastic acceleration of energetic ions can take place, as it will decrease the parameter $\kappa$ which is quite large in the plasma sheet for solar wind protons [*Ashour-Abdalla et al.*, 2009].

### 5.5. Changes With Solar Wind Pressure

[57] Increased solar wind dynamic pressure leads to a compression of the magnetosphere and the same total quantity of particles have to be distributed over a smaller volume. Consequently, the particle density/intensity will be higher and this will lead to the observed correlation. The observed differences in behavior between ~10 keV (where a correlation is evident) and >274 keV ions (no clear correlation with dynamic solar wind pressure) can be explained as follows: the plasma sheet may become thinner as result of very strong solar wind pressure, and therefore, the gyroradius versus curvature radius effect discussed above may be relevant also here.

[58] On other hand, the correlation with the solar wind dynamic pressure can be related to the Earth's ionosphere which may provide heavier ions to the magnetotail during enhanced solar wind dynamic pressure [see *Cully et al.*, 2003a; *Nosé et al.*, 2003; *Echer et al.*, 2008].

## 6. Summary

[59] Based on seven years of ion composition data from Cluster observations at radial distances $-10\ R_E < X_{GSE} < 10\ R_E$, we find the following:

[60] 1. $H^+$ intensities at ~10 keV show only a slight correlation with geomagnetic conditions (Dst and AE indices) and interplanetary magnetic field orientation. Solar wind dynamic pressure and density (i.e. effects of magnetospheric compression) seem to have a larger effect on the ~10 keV $H^+$ intensities.

[61] 2. $O^+$ ion intensities at ~10 keV are more affected by geomagnetic storms and substorms than >274 keV $O^+$ ion intensities, than their corresponding hydrogen counterparts. The >274 keV $O^+$ energization/acceleration seem to be strongest during the transition period from quiet to disturbed times, i.e., during growth phases rather than during the disturbed phases itself. The ~10 keV ions do not reveal such a dependence.

[62] 3. We find a strong positive correlation between the flux of >274 keV $O^+$, $H^+$, the $O^+/H^+$ ratio and the IMF direction. This demonstrates a connection between energy input to the magnetosphere and effective energization of energetic ions.

[63] 4. The intensity ratio between quiet and disturbed times for the ionospheric ion outflow is similar to those observed in the near-Earth magnetosphere at >274 keV. Therefore, the observed increase of the energetic ion intensity during disturbed time is not only due to a more effective acceleration but also due to enhanced ion outflow.

[64] 5. Our results seem to confirm the conclusion of *Moebius et al.* [1987] and many other studies afterwards, in that acceleration processes in the near-Earth magnetosphere are mass dependent, because it is more effective for the heavier ions ($O^+/H^+$ ratio higher).

## Appendix A: Construction of RAPID $O^+/H^+$ Ratio

[65] We shall refer to the corresponding differential particle fluxes, $j_i$, from the eight energy channels, $(E_n^{H^+}, E_n^{O^+})$, of the RAPID instrument as $j_1^{H^+}$ to $j_8^{H^+}$ and $j_1^{O^+}$ to $j_8^{O^+}$, respectively (see Table 1).

[66] The lowest energy channel for oxygen, $E_1^{O^+}$ (with energy range 84–274 keV), is contaminated by protons, and cannot be used [*Daly and Kronberg*, 2010]. The count rates in energy channels above 1 MeV (i.e., $E_6$, $E_7$ and $E_8$) are usually extremely low for both species. Useful $O^+$ channels are therefore energy channels $E_2^{O^+} - E_5^{O^+}$, covering energies from 274 to ~955 keV. For protons, corresponding to this energy range, parts of $E_4^{H^+}$ and $E_5^{H^+}$ have to be used. We have decided to use both these $H^+$ channels rather than only one $E_5^{H^+}$ and the part of the $E_2^{O^+}$, respectively, for better statistics. To construct $O^+$ and $H^+$ energy bins with matching energies, we proceed as follows:

[67] 1. Determine the integrated oxygen intensity, $J^{O^+}$, at energies from 274 up to ~955 keV. The integrated intensity is determined as the differential fluxes, $j_i^{O^+}$ multiplied by respective $\Delta E_i^{O^+}$:

$$J^{O^+} = \left(j_2^{O^+} \cdot \Delta E_2^{O^+} + j_3^{O^+} \cdot \Delta E_3^{O^+} + j_4^{O^+} \cdot \Delta E_4^{O^+} + j_5^{O^+} \cdot \Delta E_5^{O^+}\right) \cdot \left[1/\left(\mathrm{cm}^3 \cdot \mathrm{sr} \cdot \mathrm{s}\right)\right];$$

[68] 2. Obtain spectral index $\gamma$, in order to cut the part of the $E_4^{H^+}$ (see Figure A1 for illustration). For this we use fluxes from two adjacent energy channels ($E_4^{H^+}$ and $E_5^{H^+}$) and their effective energies, $E_{eff}$, the energy at which the spectrum, $A \cdot E_{eff}^{-\gamma}$, with given $A$ and $\gamma$ has the differential flux equal $J/\Delta E$:

$$\gamma = \ln\left(j_5^{H^+}/j_4^{H^+}\right)/\ln\left(E_{eff\,4}^{H^+}/E_{eff\,5}^{H^+}\right),$$

where $E_{eff}$ in this case is calculated as the geometric mean energy of the respective energy channels. See more details on these calculations in the RAPID Calibration Report [*Kronberg and Daly*, 2009, chapter B.1].

[69] 3. Determine $j_x^{H^+}$ — i.e., the $H^+$ differential flux at the virtual energy $E_x^{H^+}$, 274–374 keV (which matches the $O^+$ energy channel), with effective energy $E_{eff\,x}^{H^+} = \sqrt{274 \cdot 374}$ keV and determined $\gamma$ (see Figure A1):

$$j_x^{H^+} = j_4^{H^+} \cdot e^{-\gamma \cdot \ln\left(E_{eff\,x}^{H^+}/E_{eff\,4}^{H^+}\right)};$$

[70] 4. Determine integrated proton intensity, $J^{H^+}$, at energies from 274 up to 962 keV: $J^{H^+} = j_x^{H^+} \cdot \Delta E_x^{H^+} + j_5^{H^+} \cdot \Delta E_5^{H^+}$. With this procedure, we establish a virtual proton energy channel with the same lower energy threshold as for the oxygen. The slightly different upper energy level (962 and 948 keV, respectively) does not play any role here;

[71] 5. Define the intensity ratio: $O^+/H^+ = J^{O^+}/J^{H^+}$.

[72] In order to compare our results with other observations we need to use the energy density ratio. To establish

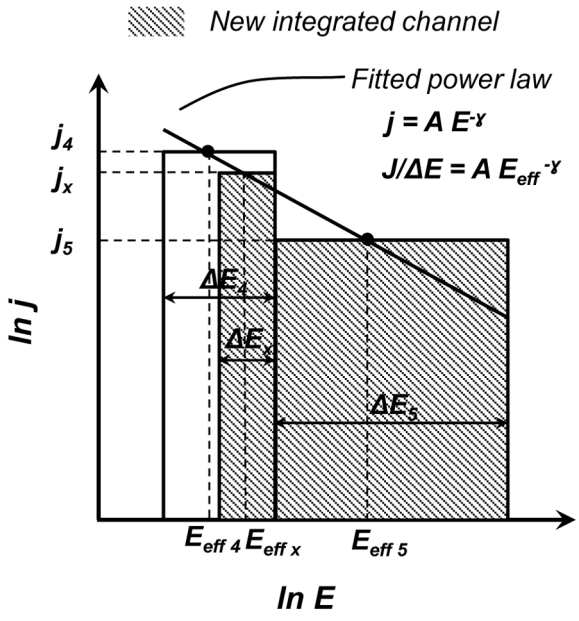


**Figure A1.** Bringing RAPID $H^+$ channels to the same energy range as $O^+$ channels: the differential flux in channels $E_4^{H^+}$ and $E_5^{H^+}$ is fitted to a power law, that fit is used to determine the differential flux, $j_x$, in the virtual channel $E_x$. $E_{eff}$ is the energy at which the spectrum with given $A$ and $\gamma$ has the differential flux equal $J/\Delta E$, where $J$ is the integrated intensity.

the energy density ratio, we assume that the relative geometric factors are correct for both species:

$$\frac{O^+}{H^+} = \frac{\pi\sqrt{2m_O}\cdot\sqrt{E_{eff}}\cdot J^{O^+}\Delta E}{\pi\sqrt{2m_H}\cdot\sqrt{E_{eff}}\cdot J^{H^+}\Delta E} = \frac{4\cdot J^{O^+}}{J^{H^+}}, \qquad \text{(A1)}$$

where $O^+ = \sqrt{m_O}\cdot\sqrt{E_{eff}}\cdot J^{O^+}$ and $H^+ = \sqrt{m_H}\cdot\sqrt{E_{eff}}\cdot J^{H^+}$.

[73] This calculation is based on the assumption that the effective energy is equal to the geometric mean of the corresponding energy thresholds. However, in our case the width of the energetic channel is quite large and this will lead to the deviation of the energy density from the value calculated using the effective energy as the geometric mean. The way to calculate this deviation one can find in the RAPID Calibration Report [*Kronberg and Daly*, 2009, chapter B.3]. The deviation is estimated to be $\sim$65% and error bar $\pm$30% from the value of the energy density calculated in equation (A1). For these calculations the typical range of $\gamma$ values derived from our data base were taken: for $O^+$ $\gamma$ = 2–3.5 and for $H^+$ $\gamma$ = 3.5–6.5. The statistical errors of the energy density and the error due to the large width of the energy channels are added in this case.

[74] **Acknowledgments.** We thank the Deutsches Zentrum für Luft und Raumfahrt (DLR) for supporting the RAPID instrument at MPS under grant 50 OC 1101. The authors are grateful for the use of the OMNI data base providing AE, Dst and solar wind parameters. E. Grigorenko thanks grants RFBR 10-02-00135; 10-02-93114; 12-02-92614 and grant of Leading Scientific Schools HIII-623.2012.2.

[75] Masaki Fujimoto thanks the reviewers for their assistance in evaluating this paper.

## References

Ashour-Abdalla, M., J.-M. Bosqued, M. El-Alaoui, V. Peroomian, M. Zhou, R. Richard, R. Walker, A. Runov, and V. Angelopoulos (2009), A simulation study of particle energization observed by THEMIS spacecraft during a substorm, *J. Geophys. Res.*, *114*, A09204, doi:10.1029/2009JA014126.

Baumjohann, W., G. Paschmann, and C. A. Cattell (1989), Average plasma properties in the central plasma sheet, *J. Geophys. Res.*, *94*, 6597–6606.

Borovsky, J. E., M. F. Thomsen, and R. C. Elphic (1998), The driving of the plasma sheet by the solar wind, *J. Geophys. Res.*, *103*, 17,617–17,640, doi:10.1029/97JA02986.

Büchner, J., and L. M. Zeleny (1986), Deterministic chaos in the dynamics of charged particles near a magnetic field reversal, *Phys. Lett. A*, *118*, 395–399, doi:10.1016/0375-9601(86)90268-9.

Chappell, C. R., T. E. Moore, and J. H. Waite Jr. (1987), The ionosphere as a fully adequate source of plasma for the Earth's magnetosphere, *J. Geophys. Res.*, *92*, 5896–5910, doi:10.1029/JA092iA06p05896.

Chappell, C. R., B. L. Giles, T. E. Moore, D. C. Delcourt, P. D. Craven, and M. O. Chandler (2000), The adequacy of the ionospheric source in supplying magnetospheric plasma, *J. Atmos. Sol. Terr. Phys.*, *62*, 421–436, doi:10.1016/S1364-6826(00)00021-3.

Cladis, J. B. (1986), Parallel acceleration and transport of ions from polar ionosphere to plasma sheet, *Geophys. Res. Lett.*, *13*, 893–896, doi:10.1029/GL013i009p00893.

Cully, C. M., E. F. Donovan, A. W. Yau, and G. G. Arkos (2003a), Akebono/Suprathermal Mass Spectrometer observations of low-energy ion outflow: Dependence on magnetic activity and solar wind conditions, *J. Geophys. Res.*, *108*(*A*2), 1093, doi:10.1029/2001JA009200.

Cully, C. M., E. F. Donovan, A. W. Yau, and H. J. Opgenoorth (2003b), Supply of thermal ionospheric ions to the central plasma sheet, *J. Geophys. Res.*, *108*(A2), 1092, doi:10.1029/2002JA009457.

Daglis, I. A., and W. I. Axford (1996), Fast ionospheric response to enhanced activity in geospace: Ion feeding of the inner magnetotail, *J. Geophys. Res.*, *101*, 5047–5066, doi:10.1029/95JA02592.

Daglis, I. A., Y. Kamide, C. Mouikis, G. D. Reeves, E. T. Sarris, K. Shiokawa, and B. Wilken (2000), "Fine structure" of the storm-substorm relationship: Ion injections during Dst decrease, *Adv. Space Res.*, *25*, 2369–2372, doi:10.1016/S0273-1177(99)00525-6.

Daly, P. W., and E. A. Kronberg (2010), RAPID products at the Cluster Active Archive, in *The Cluster Active Archive, Studying the Earth's Space Plasma Environment*, edited by H. Laakso, M. Taylor, and C. P. Escoubet, pp. 145–158, Springer, Berlin, doi:10.1007/978-90-481-3499-119.

Dandouras, I., A. Barthe, E. Penou, H. Rème, S. McCaffrey, C. Vallat, L. M. Kistler, and The Cis Team (2006), Cluster ion spectrometry (CIS) data in the Cluster active archive (CAA), *Eur. Space Agency Spec. Publ.*, *ESA SP-598*.

Echer, E., A. Korth, Q.-G. Zong, M. Fränz, W. D. Gonzalez, F. L. Guarnieri, S. Y. Fu, and H. Reme (2008), Cluster observations of $O^+$ escape in the magnetotail due to shock compression effects during the initial phase of the magnetic storm on 17 August 2001, *J. Geophys. Res.*, *113*, A05209, doi:10.1029/2007JA012624.

Escoubet, C. P., R. Schmidt, and M. L. Goldstein (1997), Cluster - science and mission overview, *Space Sci. Rev.*, *79*, 11–32.

Fu, S. Y., Q. G. Zong, T. A. Fritz, Z. Y. Pu, and B. Wilken (2002), Composition signatures in ion injections and its dependence on geomagnetic conditions, *J. Geophys. Res.*, *107*(A10), 1299, doi:10.1029/2001JA002006.

Ganguli, G., P. J. Palmadesso, J. Fedder, and A. T. Y. Lui (1995), Role of Fermi acceleration in explosive enhancement of cross-tail current in late substorm growth phase, *Geophys. Res. Lett.*, *22*, 2405–2408, doi:10.1029/95GL02488.

Glocer, A., G. Tóth, Y. Ma, T. Gombosi, J.-C. Zhang, and L. M. Kistler (2009), Multifluid Block-Adaptive-Tree Solar wind Roe-type Upwind Scheme: Magnetospheric composition and dynamics during geomagnetic storms – Initial results, *J. Geophys. Res.*, *114*, A12203, doi:10.1029/2009JA014418.

Gloeckler, G., F. M. Ipavich, B. Wilken, W. Stuedemann, and D. Hovestadt (1985), First composition measurement of the bulk of the storm-time ring current (1 to 300 keV/e) with AMPTE-CCE, *Geophys. Res. Lett.*, *12*, 325–328, doi:10.1029/GL012i005p00325.

Hamilton, D. C., G. Gloeckler, F. M. Ipavich, B. Wilken, and W. Stuedemann (1988), Ring current development during the great geomagnetic storm of February 1986, *J. Geophys. Res.*, *93*, 14,343–14,355, doi:10.1029/JA093iA12p14343.

Huber, P. J. (1981), *Robust Statistics*, pp. 107–108, John Wiley, New York.

Huddleston, M. M., C. R. Chappell, D. C. Delcourt, T. E. Moore, B. L. Giles, and M. O. Chandler (2005), An examination of the process and magnitude

of ionospheric plasma supply to the magnetosphere, *J. Geophys. Res.*, *110*, A12202, doi:10.1029/2004JA010401.

Kistler, L. M., E. Möbius, B. Klecker, G. Gloeckler, and F. M. Ipavich (1990), Spatial variations in the suprathermal ion distributions during substorms in the plasma sheet, *J. Geophys. Res.*, *95*, 18,871–18,885, doi:10.1029/JA095iA11p18871.

Kistler, L. M., D. J. Larson, E. Möbius, and W. Baumjohann (1994), The decay of superathermal ion fluxes during the substorm recovery phase, *J. Geophys. Res.*, *99*, 10,941–10,954, doi:10.1029/93JA03180.

Kistler, L. M., C. G. Mouikis, B. Klecker, and I. Dandouras (2010), Cusp as a source for oxygen in the plasma sheet during geomagnetic storms, *J. Geophys. Res.*, *115*, A03209, doi:10.1029/2009JA014838.

Kitamura, N., et al. (2010), Observations of very-low-energy (<10 eV) ion outflows dominated by $O^+$ ions in the region of enhanced electron density in the polar cap magnetosphere during geomagnetic storms, *J. Geophys. Res.*, *115*, A00J06, doi:10.1029/2010JA015601.

Kremser, G., W. Stuedemann, B. Wilken, and G. Gloeckler (1987), Observations of spatial distribution of energetic $O^{3+}$, $O^{4+}$, and $O^{5+}$ ions in the magnetosphere, *Geophys. Res. Lett.*, *14*, 685–688, doi:10.1029/GL014i007p00685.

Kronberg, E. A., and P. W. Daly (2009), Calibration report of the RAPID measurements in the Cluster Active Archive (CAA), *Tech. Rep. CAA-EST-CR-RAP*, Eur. Space Agency, Paris.

Kronberg, E. A., P. W. Daly, I. Dandouras, S. Haaland, and E. Georgescu (2010), Generation and validation of ion energy spectra based on Cluster RAPID and CIS measurements, in *The Cluster Active Archive, Studying the Earth's Space Plasma Environment*, edited by H. Laakso, M. Taylor, and C. P. Escoubet, pp. 301–306, Springer, Berlin, doi:10.1007/978-90-481-3499_120.

Lennartsson, W., and E. G. Shelley (1986), Survey of 0.1- to 16-keV/e plasma sheet ion composition, *J. Geophys. Res.*, *91*, 3061–3076, doi:10.1029/JA091iA03p03061.

Lockwood, M., J. H. Waite, Jr., T. E. Moore, C. R. Chappell, and J. F. E. Johnson (1985), A new source of suprathermal $O^+$ ions near the dayside polar cap boundary, *J. Geophys. Res.*, *90*, 4099–4116, doi:10.1029/JA090iA05p04099.

Moebius, E., M. Scholer, B. Klecker, D. Hovestadt, G. Gloeckler, and F. M. Ipavich (1987), Acceleration of ions of ionospheric origin in the plasmasheet during substorm activity, in *Magnetotail Physics*, edited by A. T. Y. Lui, pp. 231–234, The Johns Hopkins Univ. Press, Baltimore, Md.

Moore, T. E., and J. L. Horwitz (2007), Stellar ablation of planetary atmospheres, *Rev. Geophys.*, *45*, RG3002, doi:10.1029/2005RG000194.

Mouikis, C. G., L. M. Kistler, Y. H. Liu, B. Klecker, A. Korth, and I. Dandouras (2010), The $H^+$ and $O^+$ content of the plasma sheet at 15–19 Re as a function of geomagnetic and solar activity, *J. Geophys. Res.*, *115*, A00J16, doi:10.1029/2010JA015978.

Nilsson, H., et al. (2008), Transients in oxygen outflow above the polar cap as observed by the Cluster spacecraft, *Ann. Geophys.*, *26*, 3365–3373, doi:10.5194/angeo-26-3365-2008.

Nilsson, H., E. Engwall, A. Eriksson, P. A. Puhl-Quinn, and S. Arvelius (2010), Centrifugal acceleration in the magnetotail lobes, *Ann. Geophys.*, *28*, 569–576, doi:10.5194/angeo-28-569-2010.

Nosé, M., S. Ohtani, K. Takahashi, A. T. Y. Lui, R. W. McEntire, D. J. Williams, S. P. Christon, and K. Yumoto (2001), Ion composition of the near-Earth plasma sheet in storm and quiet intervals: Geotail/EPIC measurements, *J. Geophys. Res.*, *106*, 8391–8404, doi:10.1029/2000JA000376.

Nosé, M., R. W. McEntire, and S. P. Christon (2003), Change of the plasma sheet ion composition during magnetic storm development observed by the Geotail spacecraft, *J. Geophys. Res.*, *108*(A5), 1201, doi:10.1029/2002JA009660.

Nosé, M., A. Ieda, and S. P. Christon (2009), Geotail observations of plasma sheet ion composition over 16 years: On variations of average plasma ion mass and $O^+$ triggering substorm model, *J. Geophys. Res.*, *114*, A07223, doi:10.1029/2009JA014203.

Ono, Y., M. Nosé, S. P. Christon, and A. T. Y. Lui (2009), The role of magnetic field fluctuations in nonadiabatic acceleration of ions during dipolarization, *J. Geophys. Res.*, *114*, A05209, doi:10.1029/2008JA013918.

Rème, H., et al. (2001), First multispacecraft ion measurements in and near the Earth's magnetosphere with the identical Cluster ion spectrometry (CIS) experiment, *Ann. Geophys.*, *19*, 1303–1354.

Sauvaud, J. A., C. Jacquey, T. Beutier, R. P. Lepping, C. T. Russell, R. J. Belian, and A. T. Y. Lui (1996), Dynamics of the magnetospheric mid-tail induced by substorms; A multisatellite study, *Adv. Space Res.*, *18*, 35–43, doi:10.1016/0273-1177(95)00992-2.

Sharp, R. D., D. L. Carr, W. K. Peterson, and E. G. Shelley (1981), Ion streams in the magnetotail, *J. Geophys. Res.*, *86*, 4639–4648, doi:10.1029/JA086iA06p04639.

Venables, W. N., and B. D. Ripley (1999), *Modern Applied Statistics with S-PLUS*, 3rd ed., Springer, New York.

von Steiger, R., T. H. Zurbuchen, and D. J. McComas (2010), Oxygen flux in the solar wind: Ulysses observations, *Geophys. Res. Lett.*, *37*, L22101, doi:10.1029/2010GL045389.

Welling, D. T., V. K. Jordanova, S. G. Zaharia, A. Glocer, and G. Toth (2011), The effects of dynamic ionospheric outflow on the ring current, *J. Geophys. Res.*, *116*, A00J19, doi:10.1029/2010JA015642.

Wilken, B., et al. (2001), First results from the RAPID imaging energetic particle spectrometer on board Cluster, *Ann. Geophys.*, *19*, 1355–1366.

Yau, A. W., and M. Andre (1997), Sources of ion outflow in the high latitude ionosphere, *Space Sci Rev.*, *80*, 1–25, doi:10.1023/A:1004947203046.

Yau, A. W., B. A. Whalen, W. K. Peterson, and E. G. Shelley (1984), Distribution of upflowing ionospheric ions in the high-altitude polar cap and auroral ionosphere, *J. Geophys. Res.*, *89*, 5507–5522, doi:10.1029/JA089iA07p05507.

Yau, A. W., L. Lenchyshyn, E. G. Shelley, and W. K. Peterson (1985), Energetic auroral and polar ion outflow at DE 1 altitudes: Magnitude, composition, magnetic activity dependence, and long-term variations, *J. Geophys. Res.*, *90*, 8417–8432, doi:10.1029/JA090iA09p08417.

Zong, Q.-G., H. Zhang, S. Y. Fu, Y. F. Wang, Z. Y. Pu, A. Korth, P. W. Daly, and T. A. Fritz (2008), Ionospheric oxygen ions dominant bursty bulk flows: Cluster and Double Star observations, *J. Geophys. Res.*, *113*, A07S23, doi:10.1029/2007JA012764.

Zong, Q.-G., et al. (2009), Vortex-like plasma flow structures observed by Cluster at the boundary of the outer radiation belt and ring current: A link between the inner and outer magnetosphere, *J. Geophys. Res.*, *114*, A10211, doi:10.1029/2009JA014388.